Journal of Mechanical Engineering Research and Developments ISSN: 1024-1752
CODEN: JERDFO
Vol. 44, No. 4, pp. 69-83
Published Year 2021

R134a Flow Boiling Heat Transfer (FBHT) Characteristics in a Refrigeration System

Mahmood Hasan Oudah, Mohanad Kadhim Mejbel*, Mohammed Kadhim Allawi

Middle Technical University, Technical Engineering College – Baghdad, Iraq.

*Corresponding Author Email: mohanad@mtu.edu.iq

ABSTRACT

Conventional micro tubes have been widely used in the last few decades in water and air for refrigeration heat exchanger applications during evaporation or condensation. Lowering the size possibility of micro tubes drives to a higher compact and heat exchanger performance and thus reducing the charge of system's refrigerant. This research investigates the R134a pressure drop and flow boiling heat transfer measurement inside a small micro tube. In this work, a domestic refrigerator was simulated with real capacity and dimensions by designing and using a test rig refrigeration system of 310 W. A tube of 1000 mm in length made from copper horizontally oriented having 4.35 mm internal diameter representing the refrigeration's system evaporator section is adopted as a test section. A total of 36 K-type thermocouples are installed in nine locations on the copper tube's external round surface with 100 mm equal spacing. Two glass tubes are connected to the copper tube test section to visualize the R134a refrigerant in the inlet and outlet zones. A software of computational fluid dynamics (CFD) by (ANSYS Fluent 18) is employed to numerically simulate the flow boiling R134a refrigerant's heat transfer in the evaporator. This study aimed to show the influencing factors of R134a refrigerant flow boiling heat transfer (FBHT) on the designed system's evaporator experimentally and numerically. The research range is (-14 to -3) °C saturation temperature, (12.8 to 31.1) kW/m2 heat flux, (0.21 to 1) vapor quality, and (92, 160 and 187) kg/m^2.s mass flux. Experimental results reveal an improvement of 32% at 31.1 kW/m2 in the local heat transfer coefficient and 77% at 187 kg/m^2.s mass flux at constant operational testing conditions. An Enhancement of 68% in the local heat transfer coefficient when the temperature of saturation increased from (-7 to -3) °C. The average deviation between experimental and numerical results is 8%.

KEYWORDS

Phase change, Vapor quality, Evaporator, ANSYS, R134a.

INTRODUCTION

Improved technologies provide additional design options in heat transfer to increase the thermal efficiency in heat transfer units. Condensers and evaporators are leading components in cooling and heating systems. Refrigerant's thermodynamic characteristics play's a crucial condition in the heat transfer of boiling [1]. R134a is an environmentally friendly refrigerant widely used as the working fluid [2], [3]. Its flow boiling heat transfer (FBHT) is remarkable in refrigeration and air conditioning units [4]. Liquid to vapour phase change in refrigeration systems is accompanied by boiling [5]. Many researchers studied heat transfer properties for R134a FBHT in various thermal systems due to its crucial role compared with its single phase with different circular channel diameters and materials [6]–[13]. In 2016, G. B. Abadi et al. [14] mixed R25fa and R134a refrigerants and pumped the fluids in a stainless steel 3 mm ID vertically oriented 200 mm length tube to investigate the refrigerant mixture FBHT. Their boundary conditions were: heat flux (q_e) of (1 to 69) kW/m^2, and mass flux (G) of (300 to 800) kg/m^2.s. They reported that the coefficient of heat transfer (h_z) was significantly affected by G, while a minor effect occurred by altering the q_e. Y. Xu et al. conducted a study in 2016 [15] using R134a refrigerant in three smooth copper tubes of (4.065, 2.168, and 1.002) mm ID to investigate the refrigerant's h_z. Their boundary conditions were: 0.578 to 0.82 MPa saturation pressure, 18 to 35.5 kW/m^2 q_e, vapour quality of (0.03 to 1), and G of (185 to 935) kg/m^2.s. They showed that smaller ID tubes exhibited higher saturation pressures and high h_z. Besides, q_e, G, and vapour quality effects were differentiated among different tube diameters. In 2017, C. A. Dorao et al. [16] used R134a inside a 5 mm ID of stainless-steel horizontally oriented tube with 2035 mm length

to investigate the drop pressure and h_z. Their boundary conditions were: G of (200 – 400) kg/m^2.s, 18.6 °C temperature of saturation, and 3.9 to 47 kW/m^2 q_e. They reported that at high q_e, dry out vapour occurs. D. Del. Col, in 2010 [17] used an 8 mm ID tube fixed horizontally with R410A, R125, R134a, and R22 refrigerants. Their boundary conditions were: q_e of (9-53) kW/m^2, (0.07 to 0.87) vapor quality, G of (200-600) kg/m^2.s, and 25-45 °C temperature of saturation. They reported that the main elements affecting h_z were the saturation temperature and q_e, while the G had only a minor effect. In 2011, J. Kaew-On et al. [18] studied the effect of using a mini channel in heat exchangers for tubes of (1.2 and 1.1) mm ID. They used R134a refrigerant with the following conditions: q_e of (15 – 65) kW/m^2, the pressure of saturation (4 – 6) bar, and G of (300 to 800) kg/m^2.s. They concluded that h_z was mainly affected by the refrigerant's qe, with minimum G and vapour quality influence. The h_z increased by 50 – 70% when the number of channels reduced from 14 to 8. S. Basu et al. studied in 2011 [19] the h_z for R134a experimentally in (1.6 and 0.5) mm ID horizontally oriented circular tubes made from stainless steel. Their boundary conditions were: q_e of (0 - 350) kW/m^2, G of (300 - 1500) kg/m^2.s, (0 - 1) vapour qualities, and (4.9 to 11.6) bar saturation pressures. They reported that the pressure of saturation and q_e highly affected the h_z. G had a minor effect and was independent. Oh, and Son. (2011) [20] studied the h_z in an experimental investigation for R134a and R22 refrigerants flowing inside horizontal tubes made from copper of (5.35, 3.36, 1.77) mm ID. Their boundary conditions were: 10, 20, and 30 kW/m^2 heat fluxes, 0.05 to 0.97 vapor quality, G of (300 - 500) kg/m^2.s, and 0 to 5 °C saturation temperatures. They reported that smaller inner tube diameters affected the h_z. In 2009, D. Shiferaw et al. [21] conducted experiments with R134a refrigerant fluid. They used a 1.1 mm ID tube made from stainless steel, vertically oriented in their tests. Their boundary conditions were: q_e of 16 to 150 kW/m^2, the pressure of saturation (6 – 12) bar, and G of (100 – 600) kg/m^2.s. Their results showed that h_z is affected by q_e and pressure of saturation, with a minor influence on the vapour quality. D. Shiferaw et al. [22] used in 2007 (2.01 and 4.26) mm ID tubes made from stainless steel with R134a refrigerant in their experimental study. Their boundary conditions were: G of (100 - 500) kg/m^2.s, up to 0.9 vapour quality, q_e of (13 - 150) kW/m^2, and pressure of (8 – 12) bar. They concluded that using a 4.26 mm tube provided a vapour quality of (40-50) %, and a 2.01 mm tube provided (20-30) %. K. Il Choi et al. (2007) [23] conducted a multi-stage investigation on (3 and 1.5) mm ID tubes using CO2, R22, and R134a refrigerants. Their conditions were: G of (200 - 600) kg/m^2.s, q_e of (10 - 40) kW/m^2, and 10 °C temperature of saturation. They reported that q_e had a primary influence on the h_z. S. Saitoh (2005) [24] used three circular channels of 3.1, 1.12, and 0.51 mm internal diameters in their experimental study. At 0.51 mm channel diameter made the h_z proportional to q_e, with a minor influence by G. At 3.1 mm channel diameter, both G and q_e affected the h_z. In 2005, A. Greco et al. [25] researched the effect of mixed and pure refrigerants of R134a, R404A, R22, R507, and R410A on the h_z for a horizontal evaporator tube. They used a 6 m and 6 mm ID seamless stainless-steel tube. They revealed that the h_z increased with the pressure of saturation and q_e by fixing the G. They also showed that R134a provided the highest h_z among other refrigerants.

The major motivations of this paper are:

1- Showing the influence of parameters such as heat flux, vapour quality, mass flux and saturation temperature on refrigerant flow boiling heat transfer coefficient on the evaporator numerically and experimentally.
2- Analyzing the results in an evaporator tube section to predict the most influential factors that can enhance the heat transfer process.

Upon the authors best knowledge, we believe a gap in literature was found on the following points:-

- The simulated domestic refrigerator characteristic design is new.
- The specific conditions of our research were not conducted before in the Iraqi environment.
- An extensive number of K-type thermocouples were used (36 for copper tube + 12 around the system).
- Operating conditions and test tube properties (only for this specific system) is new, and.
- Computational fluid dynamics (CFD) by (ANSYS Fluent 18) software for simulating the heat transfer of this specific system numerically is also new.

This study seeks to collect data that might help and provide the literature to address these research gaps. Therefore, the purpose of this investigation is to explore:

1. The Simulation of a domestic refrigerator with real capacity and dimensions by designing and using a refrigeration system suitable for testing.
2. Studying R134a refrigerant FBHT influencing factors on the evaporator for the newly designed refrigeration system.

METHODS AND MATERIALS

Numerical Analysis

The Computational fluid dynamics software (CFD) by (ANSYS Fluent 18) was conducted in this study to simulate the R134a FBHT in the evaporator numerically. According to the presented problem, the prediction of a numerical solution by solving the governing equations is acquired to achieve excellent results in minimum effort, cost and to reduce the more challenging difficulties of experiments. R134a flow boiling analysis for a two-phase horizontal tube evaporator was studied. A numerical prediction for the h_z was made by measuring the vapour quality, refrigerant temperature, pressure, wall temperature, and flow speed distributions along the evaporator's tube length**.**

Multiphase Model

Eulerian is a two-phase flow model used in this study to analyze R134a refrigerant flow boiling. Eulerian has a good solution accuracy and a wide application range of two-phase flow problems, making it an encouraging option to adopt it in this work. Eulerian model per each phase solves Continuity, energy, and momentum equations.

Governing Equations

Some assumptions based on the two-phase properties determination and experiment results consider solving the mathematical model of the two-phase that simulates the refrigerant R134a flow boiling.

The assumptions are as the following:

The fluid is incompressible, Two-dimensional flow field, steady-state flow, q_e is uniform along the evaporator's copper tested tube wall and turbulent flow field $\vec{F}_q.\vec{F}_{lift.q}\ and\ \vec{F}_{vm.q}$ are neglected. According to the above assumptions, a reduction of the fundamental equations is acquired to the following formulas with the supplementary equations of ANSYS software [25]:

The continuity formula for phase q is:

$$\frac{\partial}{\partial t}\left(\alpha_q\,\rho_q\right)+\nabla\cdot\left(\alpha_q\rho_q\vec{v}_q\right)=\sum_{p=1}^{n}\left(\dot{m}_{pq}\right) \tag{1}$$

The momentum balance formula for phase q is:

$$\frac{\partial}{\partial t}\left(\alpha_q\rho_q\vec{v}_q\right)+\nabla\cdot\left(\alpha_q\rho_q\vec{v}_q\vec{v}_q\right)=-\alpha_q\,\nabla p+\nabla\cdot\bar{\bar{\tau}}_q+\alpha_q\rho_q\vec{g}+\sum_{p=1}^{n}\left(\vec{R}_{pq}+\dot{m}_{pq}\vec{v}_{pq}\right) \tag{2}$$

The Conservation of Energy formula for the (q) phase is:

$$\frac{\partial}{\partial t}\left(\alpha_q\rho_q h_q\right)+\nabla\cdot\left(\alpha_q\rho_q h_q\vec{u}_q\right)=\alpha_q\frac{\partial p_q}{\partial t}+\bar{\bar{\tau}}_q\cdot\nabla\,\vec{u}_q-\nabla\cdot\vec{q}_q+S_q+\sum_{p=1}^{n}\left(Q_{pq}+\dot{m}_{pq}h_{pq}\right) \tag{3}$$

k-ε Turbulence mode

Model (k-ε) was one of several methods for the treatment of turbulent flow. Because of its reliability, lower computational time, and reasonable accuracy, the standard model (k-ε) is adopted. The standard two-equation (k-ε) model allows transport equations of length scales and turbulent velocity separately determined.

The turbulence kinetic energy (k) is obtained from [25]:

$$\frac{\partial}{\partial t}(\rho k)+\frac{\partial}{\partial x_i}(\rho k u_i)\ =\frac{\partial}{\partial x_j}\left[\left(\mu+\frac{\mu_t}{\sigma_k}\right)\frac{\partial k}{\partial x_j}\right]+G_k+G_b-\rho\epsilon-Y_M+S_k \tag{4}$$

The rate of dissipation (ε), is obtained from:

$$\frac{\partial}{\partial t}(\rho\epsilon) + \frac{\partial}{\partial x_i}(\rho\epsilon u_i) = \frac{\partial}{\partial x_j}\left[\left(\mu + \frac{\mu_t}{\sigma_\epsilon}\right)\frac{\partial \epsilon}{\partial x_j}\right] + C_{1\epsilon}\frac{\epsilon}{k}(G_k + C_{3\epsilon}G_b) - C_{2\epsilon}\rho\frac{\epsilon^2}{k} + S_\epsilon \quad (5)$$

The turbulent viscosity μ_t is calculated as:

$$\mu_t = \rho C_\mu \frac{k^2}{\epsilon} \quad (6)$$

In these equations, S_k and S_ϵ of the equations (4) and (5) is a user-defined or constant source term, default is considered zero. Where σ_ϵ and σ_k Prandtl turbulent numbers for ϵ and k, Gb is the buoyancy's generation of turbulence kinetic energy. G_k is the average speed gradient's generation of turbulence kinetic energy, and Y_M is the fluctuating dilation contribution of incompressible turbulence to the overall dissipation rate.

Model constants in ANSYS software having "default" values as the following: $C_{1\varepsilon}$ = 1.44, $C_{2\varepsilon}$ = 1.92, $C_{3\varepsilon}$ = 1.3, $\sigma_k = 1$, $\sigma_\epsilon = 1.3$, and C_μ=0.09.

Boundary Conditions

Table 1 illustrates the numerical analysis's boundary conditions.

Table 1. Boundary conditions.

Wall boundary - (Constant heat flux)	
Type	Wall
Phase	Solid
Wall thickness (m)	0.001
Heat flux (W/m^2)	20000
Inlet - boundary	
Type	Velocity inlet
Phase	Mixture
Gauge pressure (Pa)	238900
Type	Velocity inlet
Phase	Phase 1
Inlet temperature (°C)	-5.5
Velocity (m/s)	2.75
Type	Velocity inlet
Phase	Phase 2
Volume fraction	0.225
Inlet temperature (°C)	-5.5
Velocity (m/s)	2.75
Outlet - boundary	
Type	Outflow

Testing Rig

Figure 1 and Table 2 show the schematic diagram and details of the experimental test rig. A water-cooling condenser is selected for the test rig for higher efficiency, more natural cooling control, and higher cooling capacity than air-cooled condensers. The refrigerant flow meters were adopted to calculate in each part the rate of flow. Three heaters were employed to simulate the refrigeration system's evaporator (test section, pre-heater, and post-heater). They were wrapped uniformly around the tube to ensure uniform q_e. Each heater was attached to a variac transformer (voltage controller) for controlling the refrigerant saturation temperature, downstream, upstream, and vapour quality of the desired test area. Three thermostats were used for the heating wires to have reasonable control over the testing rig's temperature. Two transparent tubes made from glass with the same internal diameters were fixed to the testing section at both outlet and inlet ports. Bourdon pressure gauges were installed in the system to calculate the low and high pressures of the refrigerant R134a inside the testing system. Bypass loop parallel-connected with the test section line was used to adjust the R134a G.

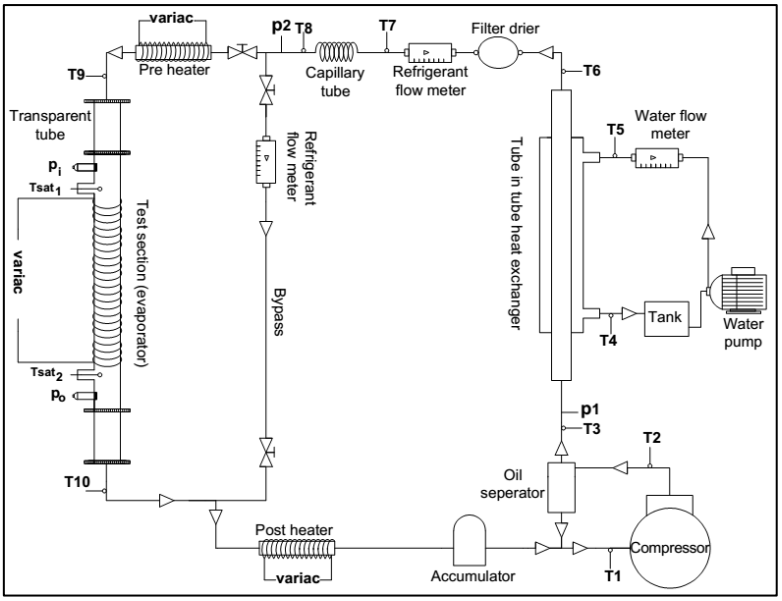

Figure 1. Refrigeration system diagram.

Table 2. The test rig components

Name	Description
Reciprocating compressor	(125W) capacity
Water-cooled condenser	Tube in tube counterflow, (1 m) length
Water pump	(20 LPM)
Water flow meter	(2-18 LPM)
Refrigerant flow meter	R134a type, 3 pieces
Capillary tube	(188 mm) length
Heating wire	3 pieces, (450W) heating resistance, (3 m) length
Glass tube	2 pieces, (180 mm) length
Variac transformer	3 pieces, rating (0 to 300 V, and 5 A)
Bourdon pressure gauge	2 pieces, range (0 to 35 bar)
K-type calibrated thermocouple	48 pieces, range (-40 to 375 ˚C)
Temperature data logger	4 pieces, PCE-T 1200 with 12 channels
Thermostat	3 pieces, (-40 to 99) ˚C Temperature range.

Testing Section

Figure 2 Illustrates the testing section. It consists of a smooth tube made from copper horizontally oriented (4.350 mm ID, 6.350 mm OD, and 1000 mm in length) representing the refrigeration's system evaporator section. A 3 m length of 450 W heat resistance wire electrically heated, wrapped uniformly around the copper test tube, was employed to provide a uniform q_e for simulating the applied thermal loading on the evaporator[26–31]. K-type thermocouples are installed in nine locations on the tube's peripheral surface with 100 mm equal distance between each site[32–34]. Four thermocouples for each section (90-degree angle between each one) are installed. To calculate the average temperature of the tube's external surface, a total of 36 thermocouples are used in the testing zone of the copper tube. Twelve other k-type thermocouples are fixed in the system in various areas, as shown in Fig. 1. The copper test tube was wrapped with insulation material to reduce the heat losses to the atmosphere caused by the heat transfer of radiation and convection. Heat flux was controlled using three variac transformers by regulating the input electric power[35–38]. Two glass tubes are connected to copper tubes to visualize the R134a refrigerant in the inlet and outlet zones during the operational tests; each glass tube is (4.35 mm ID and 180 mm length). Two thermocouple bulbs (T_{sat1} and $T_{sat2,}$ as shown in Fig.1) are installed at outlet and inlet positions of the copper tube to calculate the R134a refrigerant temperature at high accuracy.

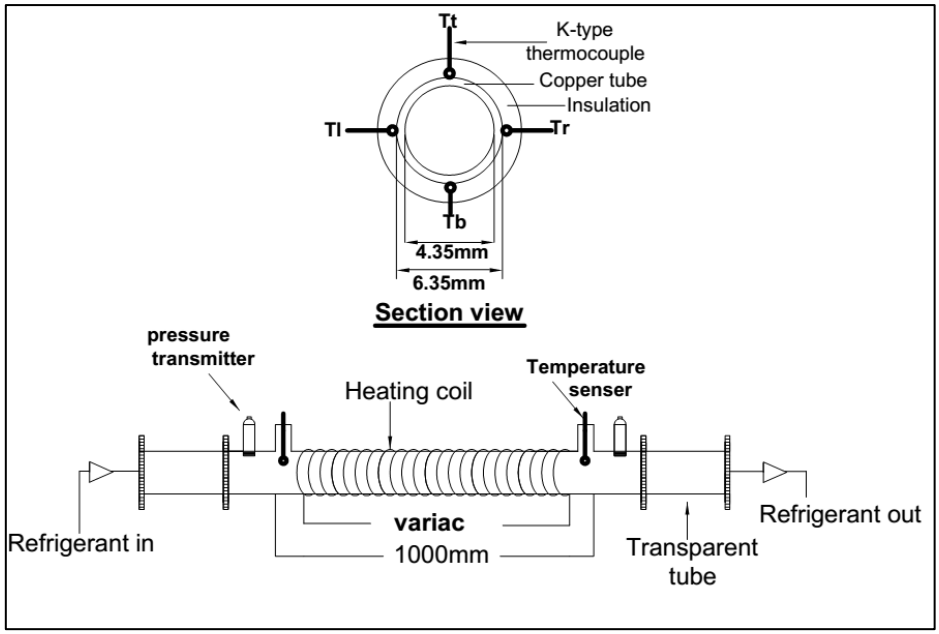

Figure 2. Illustration of the evaporator testing section.

Testing Conditions

The designed test rig's operating conditions are as follows: (-14 to -3) ˚C, (92, 160 and 187) kg/m^2.s for G, (0.21 to 1) vapor quality, and (12.8 to 31.1) kW/m^2 for q_e.

Data Reduction

Calculating the coefficient of FBHT experimentally, a series of analysis is required, and some considerations were supposed as follows:

- The q_e along copper testing tube length is uniform.
- Neglecting the axial direction heat transfer.

Coefficient of Heat Transfer

$\dot{Q}_e$ Is the rate of heat transfer determined by heating wires wrapped around the external tube surface. It is measured by:

$$\dot{Q}_e = V \cdot I \cdot \Lambda \tag{7}$$

Where Λ is the heating coefficient that represents the heat transfer process efficiency in the testing area. Λ is calculated by:

$$\Lambda = \frac{\dot{m} \cdot (h_o - h_i)}{P_{el}} \tag{8}$$

Where P_{el} is the supplied heating wire electrical power. The following formula calculates P_{el}:

$$P_{el} = V \cdot I \tag{9}$$

q_e Is the supplied heat flux from the inside copper test tube surface. The following formula calculates it:

$$\dot{q}_e = \frac{\dot{Q}_e}{\pi \cdot di \cdot L_{ts}} \tag{10}$$

The pre-heater and post-heater heat flux are calculated using equations (7, 8, 9, and 10).

h_z is the coefficient of the local heat transfer measured by Newton's cooling law:

$$h_z = \frac{\dot{q}_e}{T_{wi} - T_{sat}} \quad (11)$$

Where T_{wi} is the local temperature of the tube's inner wall, T_{sat} is the refrigerant's local temperature of saturation. Assuming radial conduction via the tube wall, T_{wi} is calculated by the following formula:

$$T_{wi} = T_{wo} - \dot{Q}_e \cdot R_w \quad (12)$$

Where T_{wo} is the local temperature of the tube's external wall. It is the average temperatures calculated around the copper test tube, as the following formula measure it:

$$T_{wo} = \frac{T_{wr} + T_{wl} + T_{wt} + T_{wb}}{4} \quad (13)$$

Where T_{wr} , T_{wl} , T_{wt} , $and\ T_{wb}$ are the copper tube wall temperatures at right, left, top, and bottom, respectively. R_w $(^{\circ}\mathrm{C/W})$ is the tube's thermal resistance calculated by:

$$R_w = \frac{Ln\left(\frac{d_o}{d_i}\right)}{2\,\pi \cdot k_{cu} \cdot L_z} \quad (14)$$

Where L_z is the copper test tube length of the test section.

$T_{sat.z}$ is the local temperature of saturation at the z position along the tested copper tube. $T_{sat.z}$ is measured concerning $P_{sat.z}$ which represents the pressure of local saturation at the z position.

$P_{sat.z}$ is calculated by the following formula:

$$P_{sat.z} = P_{i.e} - \Delta p \cdot \frac{L_z}{L_{ts}} \quad (15)$$

Where $P_{i.e}$ is the inlet refrigerant pressure. Δp is the refrigerant pressure difference between inlet and outlet ports at the testing section.

Refrigerant Vapour Quality

x_{in} is the inlet vapour quality. x_{in} is measured by:

$$x_{in} = \frac{h_{i.ts} - h_{l.i}}{h_{fg.i}} \quad (16)$$

Where $h_{fg.i}$ and $h_{l.i}$ are the specific latent and liquid heat of vaporization enthalpies respectively at the testing tube section.

$$h_{i.ts} = h_{i.p} + \frac{\dot{Q}_{pre}}{\dot{m}} \quad (17)$$

Where $h_{i.ts}$ is the inlet refrigerant's specific enthalpy, and $h_{i.p}$ is the inlet of preheater refrigerant specific enthalpy.

x_z is the refrigerant's vapour quality at a specific point, the following formula measures it:

$$x_z = x_{in} + \Delta x \cdot L_z \quad (18)$$

Where Δx is the outlet and inlet ports vapour quality difference for the tested copper tube, it is calculated using by:

$$\Delta x = \frac{x_o - x_i}{L_{ts}} \quad (19)$$

Where x_o Is the outlet refrigerant vapour quality. It is measured by:

$$x_o = \frac{h_{o.ts} - h_{Li.o}}{h_{lg.o}} \quad (20)$$

Where $h_{l.o}$ is the outlet liquid refrigerant specific enthalpy.

$h_{Lg.o}$ is the latent outlet vaporization heat of the refrigerant.

$h_{o.ts}$ Is the outlet refrigerant's specific enthalpy. It is calculated by:

$$h_{o.ts} = h_{i.ts} + \frac{\dot{Q}_e}{\dot{m}} \tag{21}$$

Measurements Uncertainly

Reliability analysis of standard errors was employed for measuring the uncertainties of the experimental results. The measurement errors in its maximum values for the instruments used in this study are ±0.04 for the local vapour quality x_z, ±3 W for the heating power q_e, h_z is ±18 W/m^2.˚C and ±0.22 bar for the local saturation pressure $P_{satz.}$

RESULTS AND DISCUSSIONS

Boiling Curve

Figure 3 illustrates the variation between the difference in wall-saturation temperature and the wall q_e for the flow boiling at -3 ˚C saturation temperature, (12.8 to 31.1) kW/m^2 q_e, and (92, 160, and 187) kg/m^2.s G. At the lowest rate of mass flow (92 kg/m^2.s), the G was affected significantly by the variation of the temperature difference and q_e. The contributions of forced convective and nucleate dominance of FBHT were visible in a temperature difference range of (12 – 43) ˚C correlated to the curve of refrigerant boiling.

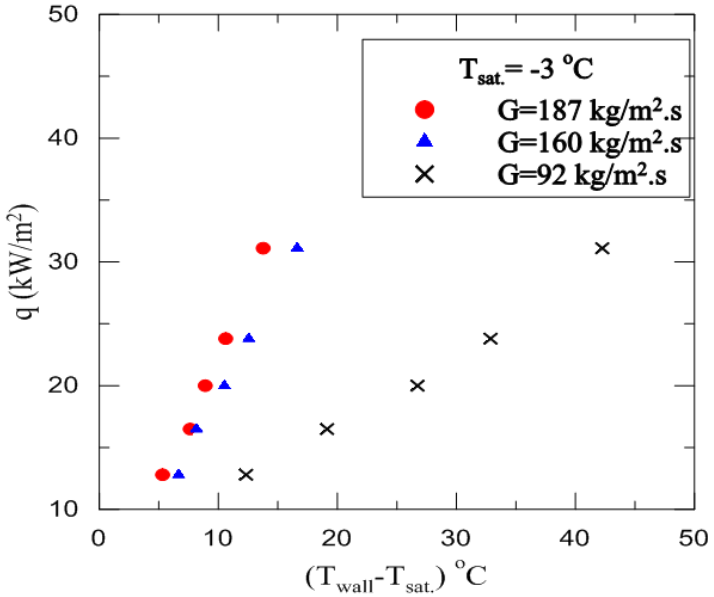

Figure 3. Wall-saturation temperature difference vs heat flux, at (-3) °C saturation temperature.

Heat Flux Effect

Figure 4 illustrates the influencce of q_e for (12.8 to 31.1) kW/m^2 at fixed mass fluxes on the h_z. A variation in h_z and vapour quality is noticed because of the convective boiling and nucleate contributions, wall refrigerant difference temperatures that correlate with the boiling curve. On q_e of 31.1 kW/m^2, the h_z was at its highest values. At constant operating conditions, the h_z increased by 32% at 31.1 kW/m^2 compared to 12.8 kW/m^2 q_e. According to Newton's law of convection, the h_z was improved at fixed differences between refrigerant temperatures and the tube surface when the q_e was increased. At G of 187 kg/m^2.s, the h_z was higher than 92 kg/m^2.s. Figure 4a and 4b had similar h_z behaviors.

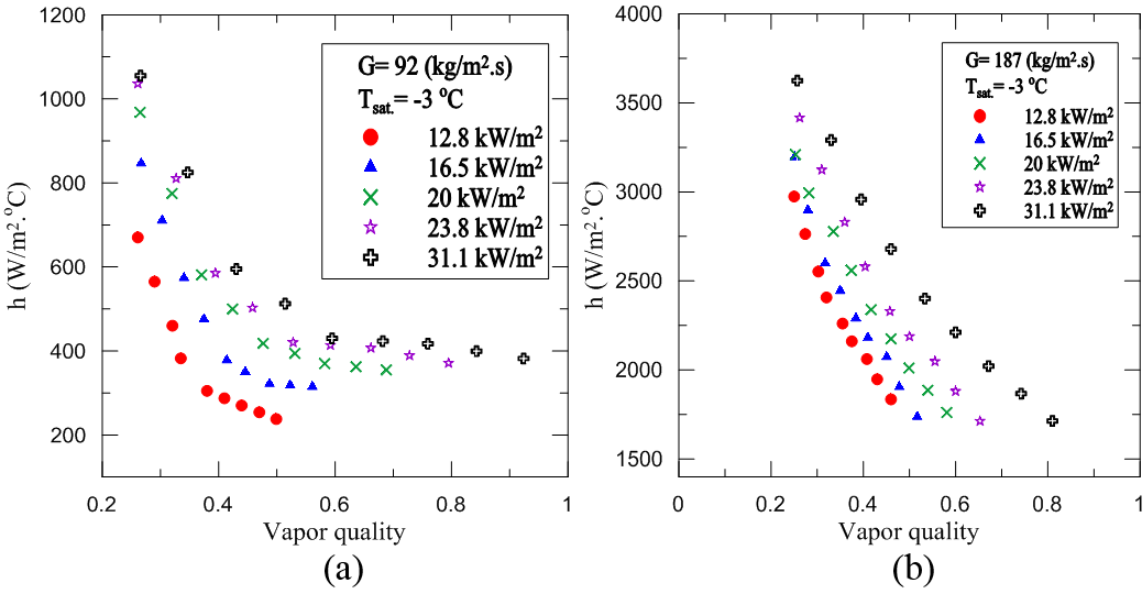

Figure 4. Vapour quality vis local coefficient of heat transfer, experimental results at the mass flux of a) 92 kg/m^2.s, b) 187 kg/m^2.s.

Mass Flux Effect

Figure 5 illustrates the G effect of (92 to 187) kg/m^2.s at fixed q_e on the h_z. A variation in the records is noticed for the vapour quality, in addition to the h_z. At G of 187 kg/m^2.s, the h_z was at its highest values for both q_e cases because of the forced convective evaporation contribution. At constant operating conditions, the h_z increased 77% at 187 kg/m^2.s compared to 92 kg/m^2.s G. Rising the applied thermal load on the evaporator copper tested tube resulted in a higher h_z at 31.1 kW/m^2 compared to 16.5 kW/m^2 q_e at other constant conditions.

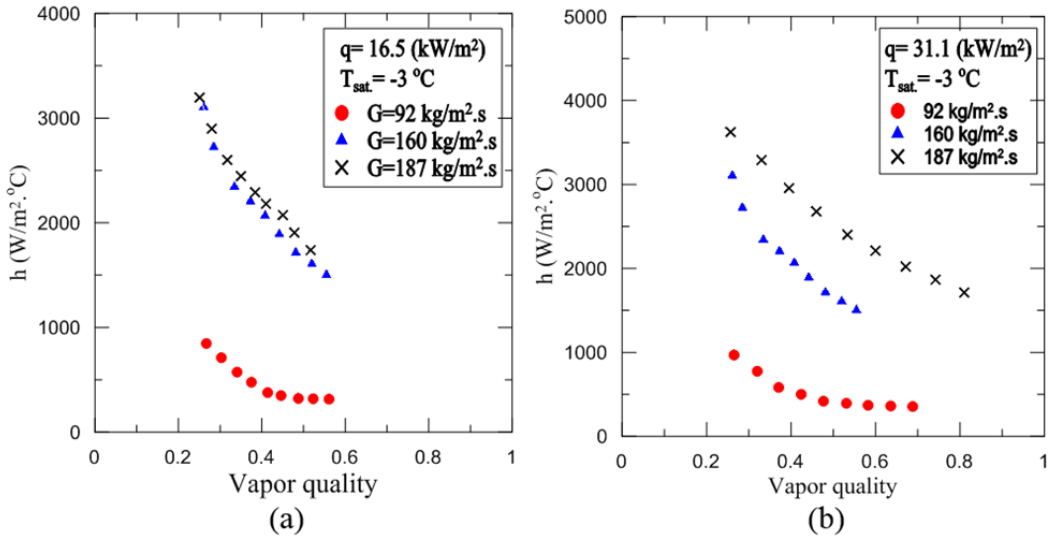

Figure 5. Coefficient of local heat transfer vs vapour quality, experimental results at a heat flux of a) 16.5 kW/m^2, b) 31.1 kW/m^2.

Heat and Mass Flux Effect

Figure 6. illustrates the effect of mass and heat fluxes with fixed testing conditions on the average h_z of the R134a flow boiling. A continuous increase in the average h_z values in the tested copper tube was noticed because of the refrigerant mass flow rate and thermal load effects. They are critical elements of the evaporator's performance. At 187 kg/m^2.s G, the average h_z was the highest among other mass fluxes.

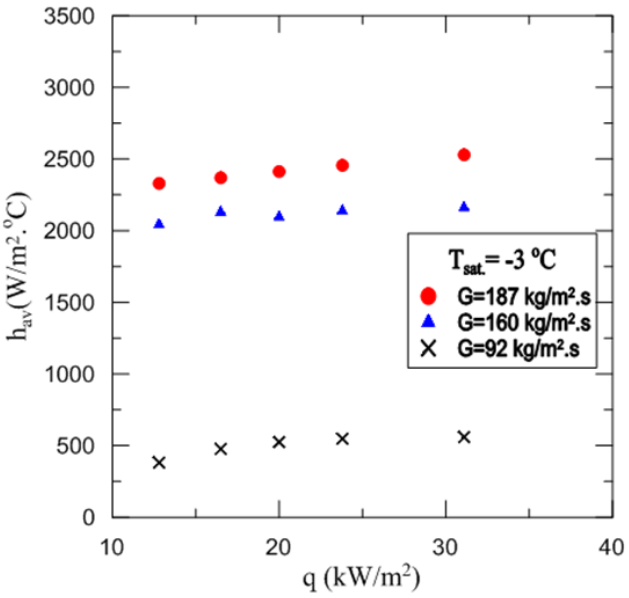

Figure 6. Average FBHT coefficient vis heat flux, experimental results at various mass fluxes.

Saturation Temperature and Inlet Vapor Quality Effect

Figure 7. illustrates the R134a saturation temperature effect at q_e of 31.1 kW/m^2 and G of 187 kg/m^2.s on the h_z. Three saturation temperatures of (-7, -3.5, and -3) °C were tested. A variation in the h_z was observed because of the increase in saturation temperatures. This behaviour was attributed mainly to the enhanced heat transfer rate at the flow boiling stratified region where the liquid film thickness inside the copper tested tube decreases causing the h_z to rise. At fixed G and q_e, an improvement of 78% for the h_z was acquired when raising the temperature of saturation from -7 to -3 °C.

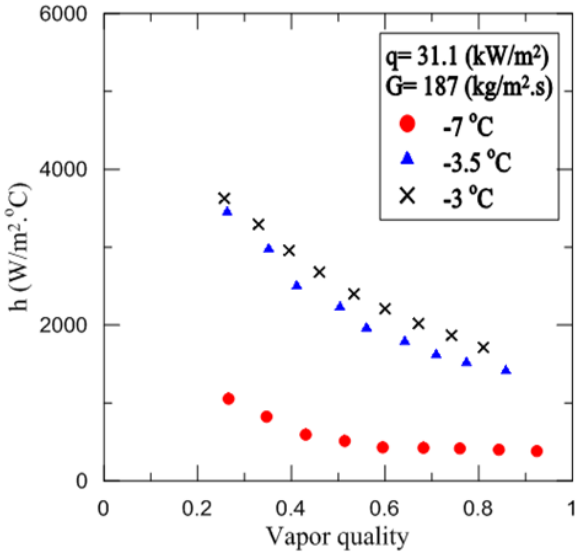

Figure 7. Vapour quality vs coefficient of local heat transfer, experimental results at a mass flux of 187 kg/m^2.s and heat flux of 31.1 kW/m^2

Figure 8. shows the h_z of the copper tested tube at fixed G and q_e affected by the inlet vapour quality of R134a. The partial increase of h_z was noticed at various inlet vapour quality values. At vapour quality of high values, the dominance is for the forced convective boiling, resulting in a partial increase of h_z.

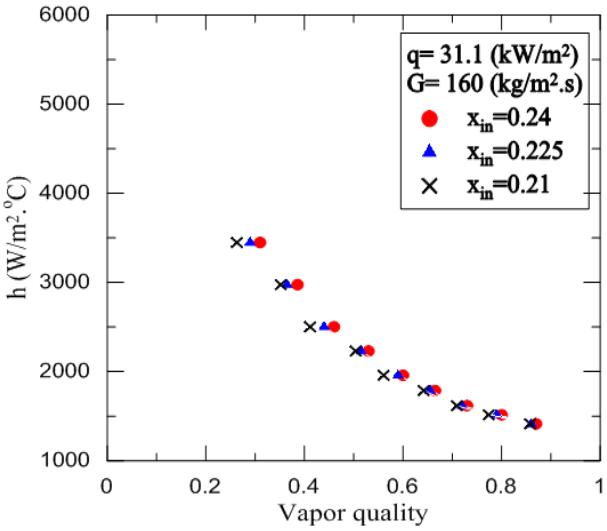

Figure 8. Vapour quality vs local heat transfer coefficient, experimental results at a mass flux of 160 kg/m^2.s and heat flux of 31.1 kW/m^2

Experimental and Numerical Comparison

Heat Flux Effect

Figure 9. illustrates the influence of q_e (12.8 to 31.1) kW/m^2 at fixed G on the h_z. The curve shows a comparison between experimental and numerical findings. At G of 187 kg/m^2.s, the h_z was higher than 92 kg/m^2.s. Numerical results show higher values than experimental results due to the refrigeration system's losses, instrument errors, humidity, fluid friction in the system, and other reasons. A deviation of 9% between the results of experimental work and numerical simulations were noticed at G of 187 kg/m^2.s and 11% at 92 kg/m^2.s

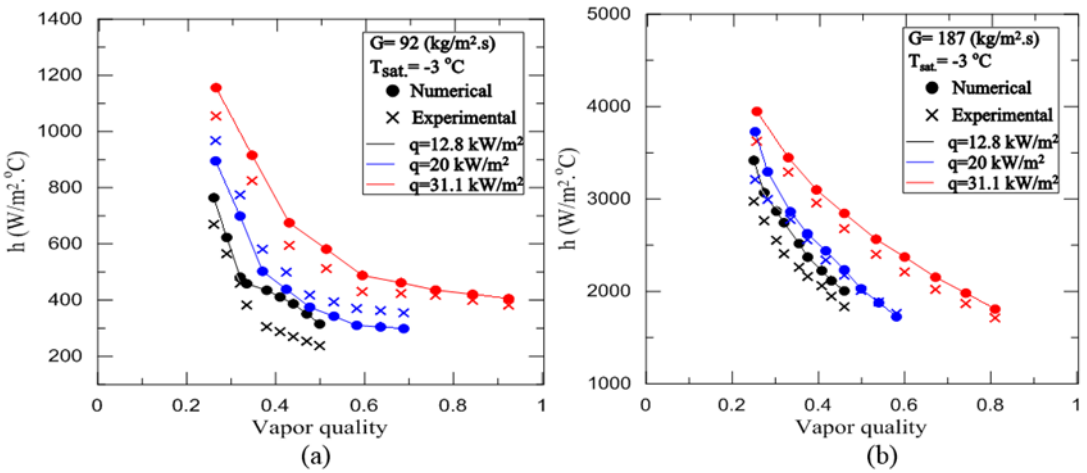

Figure 9. Heat transfer coefficient vis vapour quality at a constant mass flux of a) 92 kg/m^2. s, and b) 187 kg/m^2.s

Mass Flux Effect

Figure 10. Illustrates the effect of G (92 to 187) kg/m^2.s at fixed q_e on the h_z. The curve demonstrates the comparison of the results between numerical and experimental data. At G of 187 kg/m^2.s, the h_z was at its highest values for both q_e cases because of the forced convective evaporation contribution. Experimental results show lower values than numerical results due to the refrigeration system's losses, instrument errors, humidity, fluid friction in the system, and other reasons. A deviation between numerical and experimental results of 7% was noticed at a q_e of 31.1 kW/m^2 and 8% at 12.8 kW/m^2.

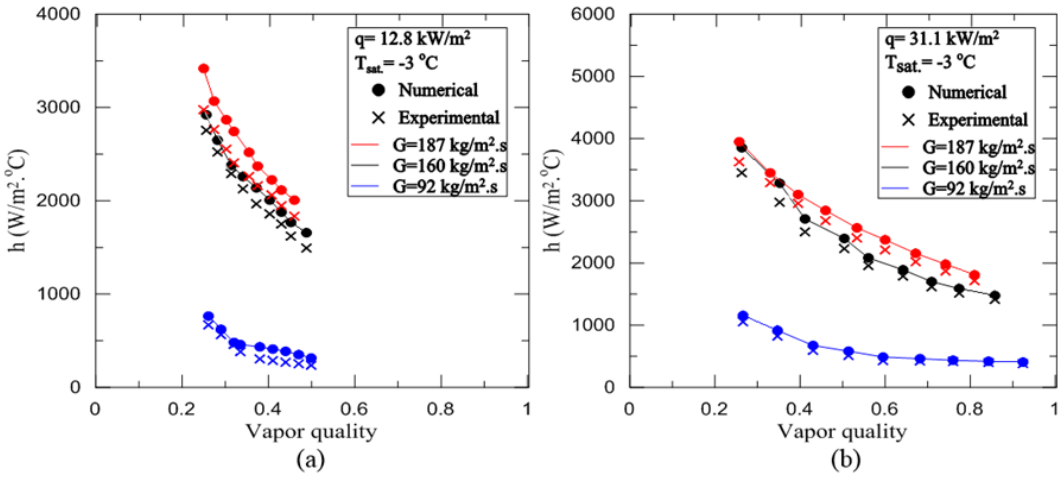

Figure 10. Coefficient of heat transfer vis vapour quality at a constant heat flux of a) 12.8 kW/m^2 and b) 31.1 kW/m^2.

Saturation Temperature Effect

Figure 11 illustrates the h_z at fixed heat and mass fluxes applying three temperatures of saturation (-7, -3.5, -3) ˚C. The curve shows a comparison between experimental and numerical findings. An average deviation between them was 9%.

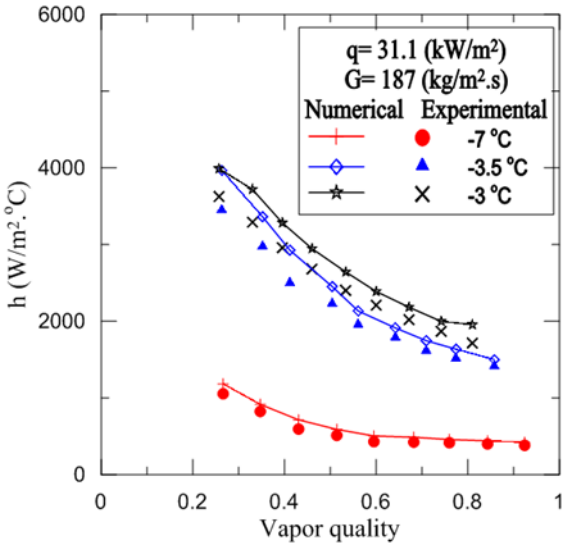

Figure 11. Coefficient of heat transfer vis vapour quality at various temperatures of saturation.

CONCLUSION

A research on the flow boiling of R134A refrigerant in one smooth tube was carried out. The effects of boiling heat transfer, saturation temperature, and mass flux were discussed. A comparison between the experimental data and predictions measured by several existing correlations using a test rig refrigeration system of 310 W was conducted. A tube of 1000 mm in length made from copper horizontally oriented having 4.35 mm internal diameter representing the refrigeration's system evaporator section is adopted as a test section. A total of 36 K-type thermocouples are in-stalled in nine locations on the copper tube's external round surface with 100 mm equal spacing. A software of computational fluid dynamics (CFD) by (ANSYS Fluent 18) is employed to numerically simulate the flow boiling R134a refrigerant's heat transfer in the evaporator.

The main conclusions can be summarized as follows:

1) Wall variation and saturation temperature difference ($T_{wall} - T_{saturation}$) are evident with lower G in the range of 92, 160, and 187 kg/m^2. s caused by various heat fluxes.
2) At constant operating conditions, the h_z increased by 32% at 31.1 kW/m^2 compared to 12.8 kW/m^2 q_e.
3) Increasing the G from (92 to 187) kg/m^2.s achieved an improvement of 77% for the h_z at constant test conditions. Since the refrigerant G is directly proportional to the h_z.
4) Increasing the temperature of saturation from (-7 to -3) $^{\circ}$C at fixed heat fluxes and refrigerant G, the h_z improved 68%.
5) A partial increment to the h_z occurred at various inlet vapour quality tested values of 0.24, 0.225, and 0.21 in the evaporator tube.
6) Good agreement within the experimental and numerical results, with an 8% average deviation.

ACKNOWLEDGMENT

The authors would like to thank the power mechanics engineering department for their kind support to accomplish this work.

REFERENCES

[1] J. Chen and W. Li, "Local flow boiling heat transfer characteristics in three-dimensional enhanced tubes," Int. J. Heat Mass Transf., Vol. 121, Pp. 1021–1032, 2018. doi: 10.1016/j.ijheatmasstransfer.2018.01.065.

[2] I. Wellid, K. Sumeru, A.A. Aziz, N. Henry, and A.M. Abioye, "Performance analysis of hydrocarbon mixture to replace R134a in an automotive air conditioning system," 2014. doi: 10.4028/www.scientific.net/AMM.554.444.

[3] B. Elhub, S. Mat, K. Sopian, A.M. Elbreki, M.H. Ruslan, and A.A. Ammar, "Performance evaluation and parametric studies on variable nozzle ejector using R134A," Case Stud. Therm. Eng., 2018. doi: 10.1016/j.csite.2018.04.006.

[4] R. Ali, B. Palm, and M.H. Maqbool, "Flow boiling heat transfer of refrigerants R134A and R245fA in a horizontal micro-channel," Exp. Heat Transf., vol. 25, no. 3, Pp. 181–196, 2012. doi: 10.1080/08916152.2011.609962.

[5] C.R. Kharangate and I. Mudawar, "Review of computational studies on boiling and condensation," International Journal of Heat and Mass Transfer. 2017, doi: 10.1016/j.ijheatmasstransfer.2016.12.065.

[6] M. Ryhl, T. Schmidt, M. Transfer, D. Version, and M. Transfer, "Flow boiling heat transfer and pressure drop characteristics of R134a , R1234yf and R1234ze in a plate heat exchanger for organic Rankine cycle units," 2017, doi: 10.1016/j.ijheatmasstransfer.2017.01.026.

[7] S. Mancin, A. Diani, and L. Rossetto, "R134a flow boiling heat transfer and pressure drop inside a 3 . 4 mm ID microfin tube," Energy Procedia, vol. 45, pp. 608–615, 2014. doi: 10.1016/j.egypro.2014.01.065.

[8] K.M.K. Pasha, "Controlling the Nusselt Number in a TiO 2 / R134a Nano-refrigerant System," vol. 37, no. 1, Pp. 179–187, 2019.

[9] C. Chen, J. Han, T. Jen, L. Shao, and W. Chen, "International Journal of Thermal Sciences Experimental study on critical heat fl ux characteristics of R134a fl ow boiling in horizontal helically-coiled tubes," Int. J. Therm. Sci., vol. 50, no. 2, Pp. 169–177, 2011. doi: 10.1016/j.ijthermalsci.2010.10.002.

[10] M.M. Mahmoud and T.G. Karayiannis, "International Journal of Heat and Mass Transfer Heat transfer correlation for flow boiling in small to micro tubes," Int. J. Heat Mass Transf., vol. 66, Pp. 553–574, 2013. doi: 10.1016/j.ijheatmasstransfer.2013.07.042.

[11] E.M. Fayyadh, M.M. Mahmoud, K. Sefiane, and T.G. Karayiannis, "International Journal of Heat and Mass Transfer Flow boiling heat transfer of R134a in multi microchannels," Int. J. Heat Mass Transf., vol. 110, Pp. 422–436, 2017. doi: 10.1016/j.ijheatmasstransfer.2017.03.057.

[12] O. Fins, T. Wen, H. Zhan, Y. Luo, and D. Zhang, "Experimental Study on the Flow Boiling Heat Transfer Characteristics in a Mini-Channel with," Pp. 1–5, 2018. doi: 10.3390/proceedings2221376.

[13] D.F. Sempértegui-tapia and G. Ribatski, "International Journal of Heat and Mass Transfer Flow boiling heat transfer of R134a and low GWP refrigerants in a horizontal micro-scale channel," vol. 108, pp. 2417–2432, 2017, doi: 10.1016/j.ijheatmasstransfer.2017.01.036.

[14] G. Bamorovat Abadi, E. Yun, and K. C. Kim, "Flow boiling characteristics of R134a and R245fa mixtures in a vertical circular tube," Exp. Therm. Fluid Sci., 2016, doi: 10.1016/j.expthermflusci.2015.11.006.

[15] Y. Xu, X. Fang, G. Li, D. Li, and Y. Yuan, "An experimental study of flow boiling heat transfer of R134a and evaluation of existing correlations," Int. J. Heat Mass Transf., 2016, doi: 10.1016/j.ijheatmasstransfer.2015.09.044.

[16] C.A. Dorao, O.B. Fernandez, and M. Fernandino, "Experimental Study of Horizontal Flow Boiling Heat Transfer of R134a at a Saturation Temperature of 18.6 °c," J. Heat Transfer, 2017. doi: 10.1115/1.4037153.

[17] D. Del Col, "Flow boiling of halogenated refrigerants at high saturation temperature in a horizontal smooth tube," Exp. Therm. Fluid Sci., 2010. doi: 10.1016/j.expthermflusci.2009.10.035.

[18] J. Kaew-On, K. Sakamatapan, and S. Wongwises, "Flow boiling heat transfer of R134a in the multiport minichannel heat exchangers," Exp. Therm. Fluid Sci., 2011. doi: 10.1016/j.expthermflusci.2010.10.007.

[19] S. Basu, S. Ndao, G.J. Michna, Y. Peles, and M.K. Jensen, "Flow boiling of R134a in circular microtubes - Part I: Study of heat transfer characteristics," J. Heat Transfer, Vol. 133, No. 5, 2011. doi: 10.1115/1.4003159.

[20] H.K. Oh and C.H. Son, "Evaporation flow pattern and heat transfer of R-22 and R-134a in small diameter tubes," Heat Mass Transf. und Stoffuebertragung, 2011. doi: 10.1007/s00231-011-0761-4.

[21] D. Shiferaw, T.G. Karayiannis, and D.B.R. Kenning, "Flow boiling in a 1.1 mm tube with R134a: Experimental results and comparison with model," Int. J. Therm. Sci., 2009. doi: 10.1016/j.ijthermalsci.2008.02.009.

[22] D. Shiferaw, X. Huo, T.G. Karayiannis, and D.B.R. Kenning, "Examination of heat transfer correlations and a model for flow boiling of R134a in small diameter tubes," Int. J. Heat Mass Transf., 2007. doi: 10.1016/j.ijheatmasstransfer.2007.07.002.

[23] K. Il Choi, A.S. Pamitran, C.Y. Oh, and J.T. Oh, "Boiling heat transfer of R-22, R-134a, and CO2 in horizontal smooth minichannels," Int. J. Refrig., Vol. 30, No. 8, Pp. 1336–1346, 2007. doi: 10.1016/j.ijrefrig.2007.04.007.

[24] S. Saitoh, H. Daiguji, and E. Hihara, "Effect of tube diameter on boiling heat transfer of R-134a in horizontal small-diameter tubes," Int. J. Heat Mass Transf., 2005. doi: 10.1016/j.ijheatmasstransfer.2005.03.035.

[25] A. Greco and G.P. Vanoli, "Flow-boiling of R22, R134a, R507, R404A and R410A inside a smooth horizontal tube," Int. J. Refrig., 2005. doi: 10.1016/j.ijrefrig.2005.01.008.

[26] M.K. Allawi, M.K. Mejbel, and M.H. Oudah, "Iraqi gasoline performance at low engine speeds," IOP Conf. Ser. Mater. Sci. Eng., Vol. 881, Pp. 12065, 2020. doi: 10.1088/1757-899x/881/1/012065.

[27] M.K. Allawi, M.K. Mejbel, Y.M. Younis, and S.J. Mezher, "A Simulation of the Effect of Iraqi Diesel Fuel Cetane Number on the Performance of a Compression Ignition Engine," Int. Rev. Mech. Eng., Vol. 14, No. 3, Pp. 151, Mar. 2020. doi: 10.15866/ireme.v14i3.18137.

[28] M. Allawi, M. Mejbel, and M. Oudah, "Variable Valve Timing (VVT) Modelling by Lotus Engine Simulation Software," Int. J. Automot. Mech. Eng., Vol. 17, No. 4 SE-Articles, Jan. 2021. doi: 10.15282/ijame.17.4.2020.15.0635.

[29] M.K. Allawi, M.H. Oudah, and M.K. Mejbel, "Analysis of Exhaust Manifold of Spark-Ignition Engine By Using Computational Fluid Dynamics (CFD)," J. Mech. Eng. Res. Dev., Vol. 42, No. 5, Pp. 211–215, 2019.

[30] M.K. Allawi, M.K. Mejbel, Y.M. Younis, and S.J. Mezher, "A Simulation of the Effect of Iraqi Diesel Fuel Cetane Number on the Performance of a Compression Ignition Engine," Int. Rev. Mech. Eng., Vol. 14, No. 3, Pp. 151–159, Mar. 2020. doi: https://doi.org/10.15866/ireme.v14i3.18137.

[31] M.K. Mejbel, M.K. Allawi, and M.H. Oudah, "Effects of WC, SiC, iron and glass fillers and their high percentage content on adhesive bond strength of an aluminium alloy butt joint: An experimental study," J. Mech. Eng. Res. Dev., Vol. 42, No. 5, Pp. 224–231, 2019. doi: 10.26480/jmerd.05.2019.224.231.

[32] S.J. Mezher, M.O. Dawood, O.M. Abdulmunem, and M.K. Mejbel, "Copper doped nickel oxide gas sensor," Vacuum, Vol. 172, Pp. 109074, 2020, doi: 10.1016/j.vacuum.2019.109074.

[33] S.J. Mezher, M.O. Dawood, A.A. Beddai, and M.K. Mejbel, "NiO nanostructure by RF sputtering for gas sensing applications," Mater. Technol., Aug., 2019, doi: 10.1080/10667857.2019.1653595.

[34] S.J. Mezher, K.J. Kadhim, O.M. Abdulmunem, and M.K. Mejbel, "Microwave properties of Mg–Zn ferrite deposited by the thermal evaporation technique," Vacuum, Vol. 173, Pp. 109114, 2020, doi: 10.1016/j.vacuum.2019.109114.

[35] W.J. Aziz, M.A. Abid, D.A. Kadhim, and M.K. Mejbel, "Synthesis of iron oxide (β-fe2o3) nanoparticles from Iraqi grapes extract and its biomedical application," IOP Conf. Ser. Mater. Sci. Eng., Vol. 881, Pp. 12099, 2020, doi: 10.1088/1757-899x/881/1/012099.

[36] T.H. Abood Al-Saadi, S. Hameed Mohammad, E.G. Daway, and M.K. Mejbel, "Synthesis of intumescent materials by alkali activation of glass waste using intercalated graphite additions," Mater. Today Proc., 2021, doi: https://doi.org/10.1016/j.matpr.2020.12.228.

[37] A.R. Baqer, A.A. Beddai, M.M. Farhan, B.A. Badday, and M.K. Mejbel, "Efficient coating of titanium composite electrodes with various metal oxides for electrochemical removal of ammonia," Results Eng., Vol. 9, Pp. 100199.

[38] T.H.A. Al-Saadi, E.G. Daway, S.H. Mohammad, and M.K. Mejbel, "Effect of graphite additions on the intumescent behaviour of alkali-activated materials based on glass waste," J. Mater. Res. Technol., Vol. 9, No. 6, Pp. 14338–14349, 2020.